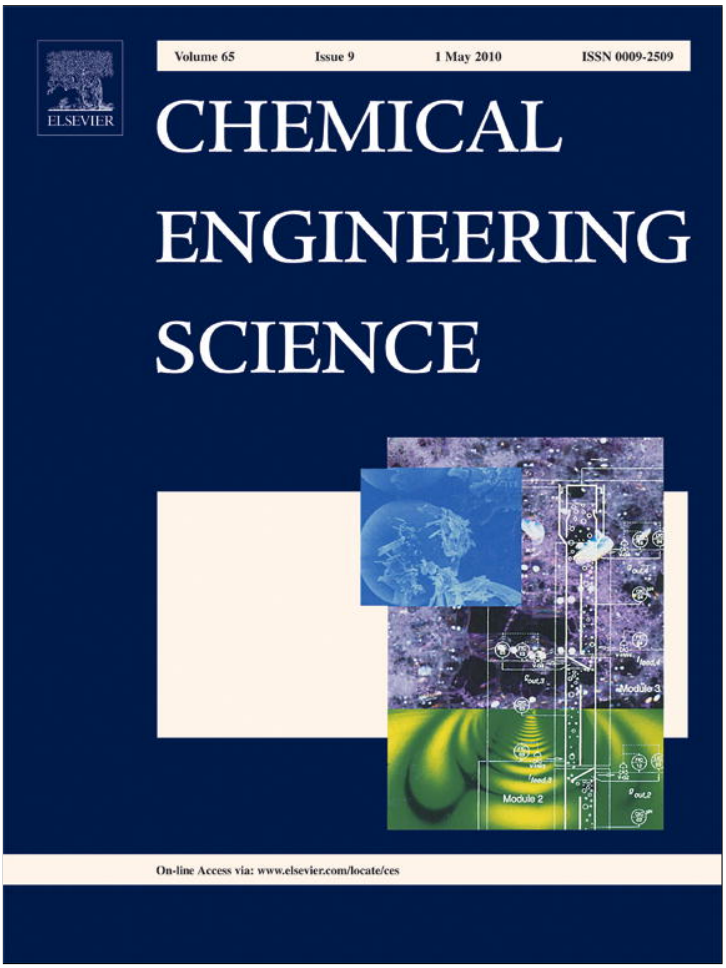

Chemical Engineering Science 65 (2010) 2835–2846

Contents lists available at ScienceDirect

Chemical Engineering Science

journal homepage: www.elsevier.com/locate/ces

A semi-analytical model for gas flow in pleated filters

M. Rebaï [a,b], M. Prat [a,b,*], M. Meireles [c], P. Schmitz [d,e,f], R. Baclet [g]

[a] Université de Toulouse; INPT, UPS; IMFT, Avenue Camille Soula-F 31400, France
[b] CNRS, IMFT-F 31400, France
[c] Laboratoire de Génie Chimique 118 route de Narbonne, 31062 Toulouse cedex, France
[d] Université de Toulouse; INSA,UPS,INP; LISBP, 135 Avenue de Rangueil, F-31077 Toulouse, France
[e] INRA, UMR792 Ingénierie des Systèmes Biologiques et des Procédés, F-31400 Toulouse, France
[f] CNRS; UMR5504, F-31400 Toulouse, France
[g] Mecaplast Group, Parc d'Activité de la Croisette, Rue des Poissonniers, 62300 Lens, France

ARTICLE INFO

Article history:
Received 17 February 2009
Received in revised form
11 January 2010
Accepted 15 January 2010
Available online 20 January 2010

Keywords:
Gas filtration
Fibrous materials
Pleated filters
Modelling
CFD simulation

ABSTRACT

A semi-analytical model of gas flow in pleated fibrous filters is developed for large filtration velocities. This case presents two main new and distinguishing features compared to the low filtration velocity situations studied in previous works: the velocity profiles are not parabolic within the pleat channels and the filtration velocity is not uniform along the pleated filter element and this has a great impact on the filter loading. The model relies on similarity solutions to the Navier–Stokes equations in the channels formed by pleating the filter medium. After validation by comparison with direct CFD simulations and experimental data, the model is used to determine the optimal pleat density, i.e. the pleat density minimizing the overall pressure drop across the filter for given flow rate, pleat length and given filter medium properties. As illustrated in the paper, this model greatly facilitates the study of flow within the pleated filter compared to a standard CFD approach. It represents an excellent basis for the more involved problem of filter loading computation. In particular, no remeshing across the width of the pleated filter entrance channels is needed when a filtration cake forms at the channel walls.

1. Introduction

Air filtration pleated filters are commonly encountered in various applications related notably to nuclear or automotive industry. Our general objective in this context is to develop a numerical tool for simulating the process of air filtration through pleated fibrous filters. This tool is developed in order to reduce the design time, the number of trials as well as to optimize the filter geometry (transport properties, pleat length and density, impact of filter supply and exit pipes position and sizes, etc.). It should be able to perform accurate predictions of the filter global pressure drop before clogging as well as its variations during the clogging phase (not considered in the present work).

Computing the flow within the filter solving directly the Navier–Stokes equations is possible, e.g. Subrenat et al. (2003), Nassehi et al. (2005), but computational time consuming. Although useful for example to validate a simplified approach, direct CFD simulations are therefore not particularly well adapted for efficient optimization studies. It is therefore attractive to develop simplified numerical approaches so as to considerably increase the efficiency of numerical simulations in this context.

As schematically illustrated in Fig. 1, different scales can be distinguished. The first scale is the fibre scale. The second scale is that of the filter medium, a fibrous material in our case. The third scale is the pleat scale. At this scale, the objective is to compute the flow inside the pleats as well as the overall pressure drop across a pleated filter element for a given flow rate. The fourth scale (not shown in Fig. 1) is the filter scale, i.e. the scale of the cartridge or the filter placed within the engine air supply line. In the present work, we concentrate on the third scale, i.e. the pleat scale. The flow configuration studied as well as a sketch of representative unit elements of pleated filter are depicted in Fig. 2. As shown in Fig. 2, the average direction of the flow is perpendicular to the filter element. The fluid (gas in our case) enters the filter element through the inlet of the pleat entrance channels, flows through the fibrous materials separating the entrance channels from the pleat exit channels and quits the filter element through the outlet of the pleat exit channels. Owing to the symmetries of this system, the study can be performed over the reduced domains shown in Fig. 2. In particular, we are interested in predicting the net pressure drop across a filter panel as functions of filter medium properties, average flow rate, pleat density (number of pleats per unit width), pleat shape and pleat length.

* Corresponding author at: Université de Toulouse; INPT, UPS; IMFT, Avenue Camille Soula-F 31400, France. Tel.: +33 561 28 58 83; fax: +33 561 28 58 99.
E-mail address: prat@imft.fr (M. Prat).

0009-2509/$ - see front matter © 2010 Elsevier Ltd. All rights reserved.
doi:10.1016/j.ces.2010.01.014

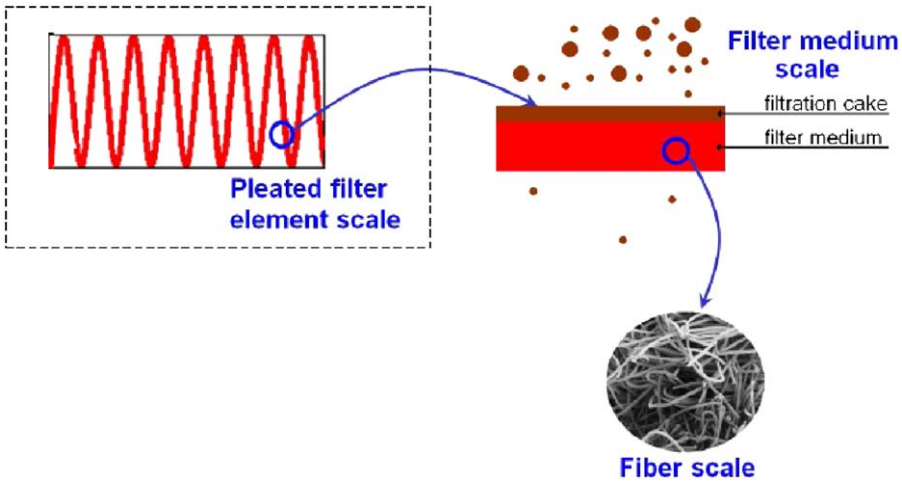

Fig. 1. Three scales of interest for the analysis of filtration in a filter. In this work, we concentrate on the pleated filter element scale (box with the dashed frame).

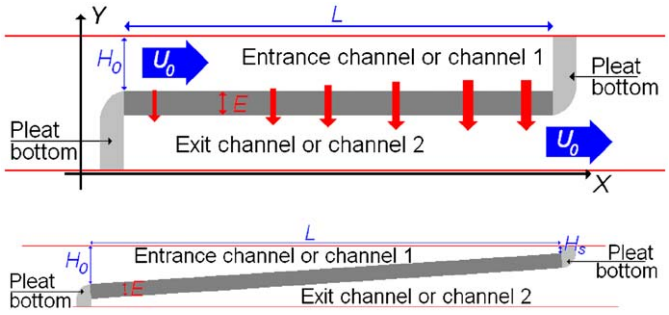

Fig. 2. Uniform and non-uniform model pleats. The regions in grey correspond to the porous medium (in light grey for the pleat bottoms and in darker grey elsewhere along the pleat). The red arrows schematize the flow through the porous medium whereas the blue arrows are for the flow in the entrance and exit channels. (For interpretation of the references to the colour in this figure legend, the reader is referred to the web version of this article.)

The methodology used to derive our simplified model is based on the spatial averaging of the flow equations over the cross-section of the entrance or exit pleat channel and takes advantage of the similarity properties of the pressure and velocity profiles within the pleat channels. This type of methodology has already been applied successfully to filtration problems, e.g. Oxarango et al. (2004), including pleated filters, Benmachou et al. (2003), Benmachou (2005), but for relatively low filtration velocities. In the application motivating our study, i.e. air filtration in automotive filters, the flow conditions are markedly different owing to much higher filtration velocities and this implies reconsidering the modelling. The flow in such systems is usually characterized by the filtration Reynolds number Re_w defined as $\mathrm{Re}_w = \rho \langle V_w \rangle H_0/\mu$, where ρ, $\langle V_w \rangle$, H_0 and μ are the fluid density, average filtration velocity through the filter medium, channel half-width at the inlet of entrance channel and fluid dynamic viscosity respectively, and the channel Reynolds number $\mathrm{Re}_0 = \rho \langle U_0 \rangle H_0/\mu$, where $\langle U_0 \rangle$ is the average longitudinal (=in the x direction) velocity component at the inlet of the pleat entrance channel, see Fig. 2. In the liquid filtration problem considered for example in Benmachou et al. (2003), Benmachou (2005), Re_w and Re_0 are typically lower than 0.6 and 10, respectively. In contrast, Re_w and Re_0 are in the ranges [20, 200] and [100, 2000] respectively in the gas filtration problem considered here. As a result, the gas filtration problem studied in this paper presents at least two distinguishing features. Contrary to the cases considered in previous works, see also Lücke and Fissan (1996), the velocity profiles within the pleat are not parabolic but much more flat, e.g. Terrill (1965). Second, the filtration velocity varies along the pleat channels, whereas a uniform filtration velocity can be generally assumed for lower filtration velocities.

Our model is based on the assumption that the known similarity solution for large uniform injection (resp. suction) rates in a porous channel, Terrill (1965), Brady (1984), represents a reasonable local approximation to the Navier–Stokes equations solution in the pleat entrance (resp. exit) channel.

The model applies to pleats of uniform width as well as to pleats of varying width. The computations reported in this paper have been performed for the two types of pleated filter model element depicted in Fig. 2. The first one is characterized by an uniform channel width, whereas the second is characterized by an entrance (resp. exit) channel decreasing (resp. increasing) width. Note the definition of the geometrical parameters defining the geometry of each model pleat in Fig. 2. The uniform pleat configuration is a model situation interesting from a modelling standpoint (equations are simpler) and as an intermediate step in the comparison with CFD but it is not necessarily representative of real systems. The most interesting case for the applications is clearly when the pleat aperture varies along the pleat. Also, the pleat aperture changes during the filter loading when a filtration cake forms at the channel walls. Hence, it is important to consider pleats of varying width if one is willing to simulate the filter loading, e.g. Rebai et al. (2009).

Note also that a distinction is made between the pleat bottom region (in light grey in Fig. 2) and the remaining part of the pleat wall (darker grey in Fig. 3). In fact, consideration of the pleat filter making process suggests that the filter medium permeability and thickness are different in the pleat bottom region from their values elsewhere along the pleat channels owing to the compression of the fibrous materials when the pleated filter panel is formed from a flat layer of fibrous material. We expect that the particular values of fibrous material local permeability in the pleat bottom region range between two extremes: a very small permeability, i.e. a non-porous material, and the same permeability as for the flat fibrous material. These two cases will be referred to as the cases with impervious pleat bottoms and with full porous pleat bottoms, respectively.

The paper is organized as follows. In Section 1, the validity of the similarity solutions in pleated filters for a large average filtration velocity is explored. The mathematical developments leading to the modelling of flow in terms of a system of four coupled ODEs are summarized in Section 2. In Section 3, results of simulation are

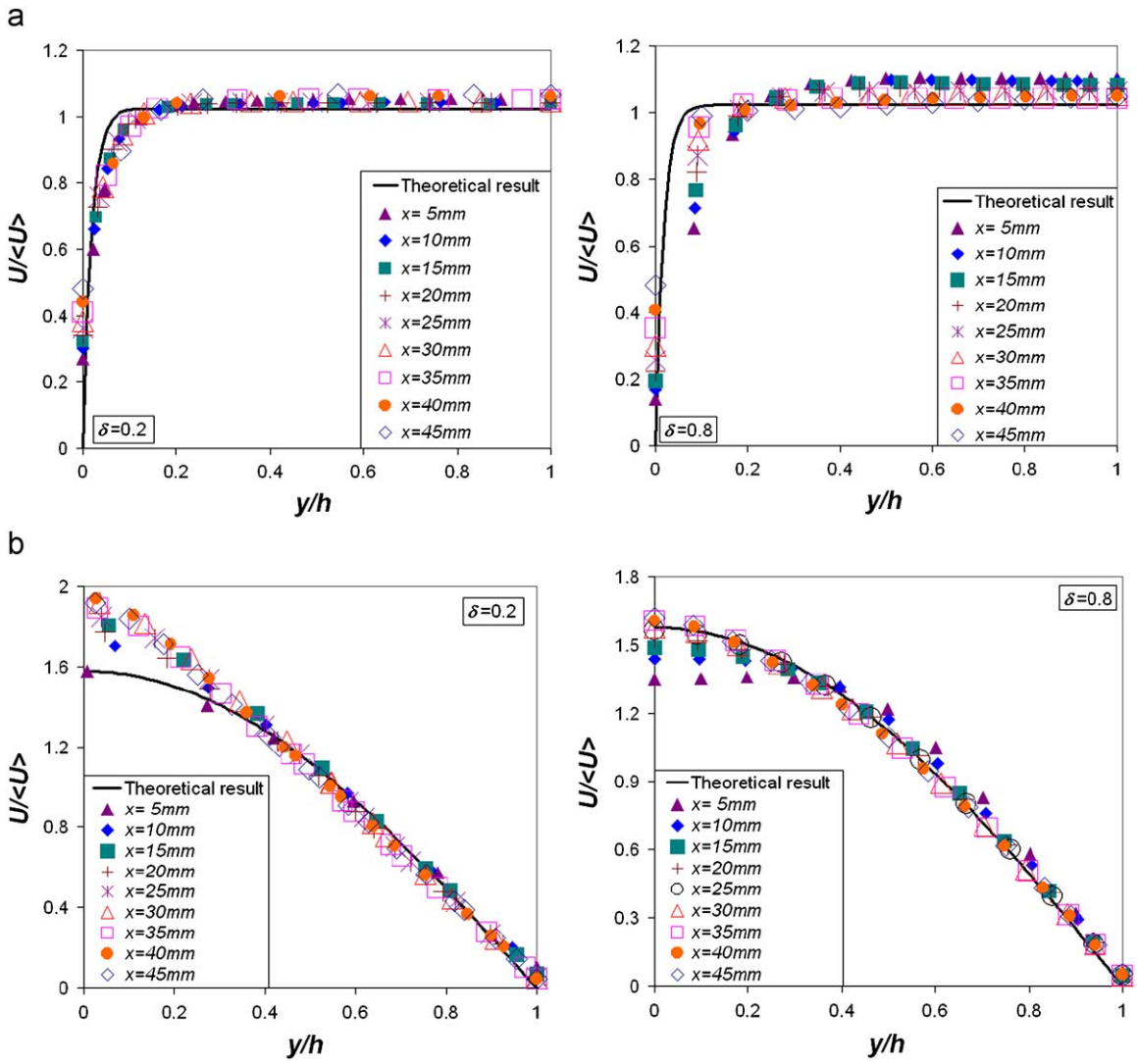

Fig. 3. Evolution of the longitudinal velocity component U for impervious pleat bottoms at various location X along the pleat channels; $\langle U \rangle$ is the spatial average of U over the half-width channel h. Comparison of the analytical solution for a uniform velocity filtration (solid line, Terrill, 1964 and Terrill, 1965) and CFD simulation results for pleats of variable width (symbols). Calculations are for a pleated filter of pleat density 8 pleats/100 mm and pleat height of 51 mm. The thickness of fibrous medium is 1.45 mm and its permeability is 3.56×10^{-10} m^2. The averaged filtration velocity is 0.39 m/s. $\delta = H_s/H_0$ (see Fig. 3): (a) entrance channel, (b) exit channel.

compared with experimental results and direct CFD simulations whereas the optimal number of pleats, i.e. the pleat density minimizing the pressure drop for a given flow rate, is studied in Section 4.

For simplicity and clarity, the dimensionless variables are written with lowercase letters whereas uppercase letters are used for the dimensional variables.

2. Similarity solutions in pleated filters

As mentioned in the Introduction, similarity solutions to the Navier–Stokes equations have been thoroughly investigated for uniform channels with porous walls and an uniform injection or suction velocity along the walls, Berman (1954), Terrill (1964, 1965). This leads to express the velocity profiles in dimensionless form (using the channel half-width, H_0, and the average longitudinal velocity component at the entrance of the entrance channel, $\langle U_0 \rangle$, as characteristic length and velocity) as

$$u(x,y) = \langle u(x) \rangle f'(y/h) \tag{1}$$

$$v(x,y) = \frac{\mathrm{Re}_w}{\mathrm{Re}_0} f(y/h) \tag{2}$$

where h is the local channel half-width, $\langle u(x) \rangle$ is the averaged velocity in the channel, which is defined as

$$\langle u(x) \rangle = \frac{1}{h} \int_0^h u(x,y)\, dy \tag{3}$$

The similarity function f is governed by a fourth-order non-linear differential equation which can be solved analytically, Berman (1954), Terrill (1964, 1965). For the large suction rates that are of interest for our study, f reads

$$f = 1 + \frac{1}{\mathrm{Re}_w - 1} f_1 + \frac{1}{(\mathrm{Re}_w - 1)^2} f_2 + \frac{1}{(\mathrm{Re}_w - 1)^3} f_3 \tag{4}$$

with

$$f_1(z) = 1 - e^{-\mathrm{Re}_w z} - \mathrm{Re}_w z \tag{5}$$

$$f_2(z) = \left(-\frac{1}{2} \mathrm{Re}_w^2 z^2 - 3\,\mathrm{Re}_w z \right) e^{-\mathrm{Re}_w z} - \mathrm{Re}_w z + \frac{3\,\mathrm{Re}_w (1 - z - e^{-\mathrm{Re}_w z})}{\mathrm{Re}_w - 1} \tag{6}$$

$$f_3(z)=\left(-\frac{1}{8}\,\mathrm{Re}_w^4 z^4-\frac{3}{2}\,\mathrm{Re}_w^3 z^3-8\,\mathrm{Re}_w^2 z^2-22\,\mathrm{Re}_w z\right)e^{-\mathrm{Re}_w z}+\frac{1}{4}e^{-2\mathrm{Re}_w}+\frac{11\,\mathrm{Re}_w z}{\mathrm{Re}_w z-1}\left(\frac{1-z}{2}-e^{-\mathrm{Re}_w z}\right) \tag{7}$$

where $z=1-y/h(x)$

whereas the expression of f for large injection rates reads

$$f=f_0+\varepsilon f_1 \tag{8}$$

$$f_0(y)=\sin(z) \tag{9}$$

$$f_1(y)=\frac{\pi}{4}(\sin(z)-z\cos(z))\left|\ln\left(\tan\left(\frac{z}{2}\right)\right)\right|+\left(\int_0^z\frac{\theta}{\sin\theta}\,d\theta-\frac{2}{\pi}Az\right)\frac{\pi}{4}\cos(z) \tag{10}$$

where

$$z=\frac{\pi}{2}\frac{y}{h},\quad \varepsilon=-\frac{\pi}{2\,\mathrm{Re}_w},\quad A=\int_0^{\pi/2}\frac{\theta}{\sin\theta}\,d\theta-1.$$

Eqs. (8)–(10) correspond in fact to the outer solution as discussed in Terrill (1965). This solution is obtained under the assumption that the inertia term is dominant over the viscous term, which is not correct in the centre of the channel for high blowing rates. The flow in the channel central region is given by the inner solution, which reads

$$f(y)=z-\frac{z^3}{6}+\varepsilon\left(\frac{\pi A-2}{4}\right)z-\frac{z^3}{12}\varepsilon\ln\varepsilon-\frac{z}{4}\varepsilon^2\ln\varepsilon \tag{11}$$

noting that the inner layer has a thickness of $O(\varepsilon^{1/2})$.

The flow in the entrance (resp. exit) channel of a pleated filter is *a priori* different from the flow corresponding to the above solutions since the suction (resp. injection) velocity is not uniform (see below) and also because the channels width is generally not constant. However, it turns out that the above similarity solutions represent a reasonable approximation to the flow in the channels of the pleated filter. This is shown in what follows from direct CFD simulations of the flow in the pleated filter channels. The CFD simulations have been performed using the commercial code Fluent™ by solving the Navier–Stokes (NS) equations in the entrance and exit channels. More precisely the problem solved numerically with Fluent™ in the entrance and exit channels can be expressed in dimensionless form as

$$\nabla\cdot\mathbf{u}=0. \tag{12}$$

$$\mathbf{u}\cdot\nabla\mathbf{u}=-\nabla p+\frac{1}{\mathrm{Re}_0}\nabla^2\mathbf{u} \tag{13}$$

where as before, U_0 and H_0 are used as characteristic velocity and length whereas ρU_0^2 is used as characteristic pressure. In the fibrous material region, Darcy's law is used. Hence the CFD software allows solving the NS equations in the free fluid zone coupled with Darcy's law in the porous wall. Further details on the direct CFD computational aspects are presented in Appendix A. The use of Darcy's law for describing the flow within the porous walls is supported by the following order of magnitude analysis, considering the "fibre" Reynolds number defined by $\mathrm{Re}_f=\rho d_f\langle V_w\rangle/\phi\mu$, where Φ is the filtration medium porosity. The fibre diameter d_f is typically in the range [15–30] μm in the applications motivating the present work whereas the average filtration velocity is at most 0.65 m/s and the maximum filtration velocity considered in this paper is 1.5 m/s (see Fig. 5). This leads to $\mathrm{Re}_f\approx 1.3$ and $\mathrm{Re}_f\approx 3$ respectively with d_f=30 μm. It is well know that Darcy's law can be safely used as long as $\mathrm{Re}_f\le 1$, and that inertia effects become noticeable in the range $\mathrm{Re}_f\approx 1-10$, e.g. Dullien (1992). The deviation from linearity is however rather weak for $1\le\mathrm{Re}_f\le 3$. It should also be noted that the main contribution to the overall pressure loss is not due to the porous medium but to the pressure loss in the channels. Hence a small error in the computation of the porous medium contribution has a very small impact on the overall pressure drop. Therefore it can be concluded that Darcy's law represents here a quite reasonable approximation. For applications involving higher fibre Reynolds number, it would be straightforward to extent our model adopting Forchheimer's equation, e.g. Subrenat et al. (2003), Li (2009) and references therein, in place of Darcy's law.

The similarity of the NS equations solution obtained with the CFD commercial software has been studied for the two filter elements depicted in Fig. 2, various representative values of fibrous medium permeability and pleat geometrical parameters, several values of Re_w and Re_0 representative of gas filtration and for impervious as well as permeable pleat bottoms, Rebai (2007). For every case studied, the agreement was good to excellent between the CFD simulations and the similarity solutions proposed by Terrill (1965). Note that only the outer solution, Eq. (5), has been compared to the CFD results as far as the exit channel is concerned.

Representative examples of the comparison with CFD are depicted in Fig. 3. The results shown in Fig. 3 are for pleats of variable width. The geometrical parameter δ is defined as $\delta=H_s/H_0$, see Fig. 3. Hence for a given pleat length, the width channel variation is more pronounced for a small δ. The results of Fig. 3 are for a pleat length L=51 mm, a pleat density of 8 pleats/100 mm (which corresponds to H_0=4.0 mm for δ=0.2 and H_0=2.67 mm for δ=0.8), and a fibrous material thickness E and permeability K equal to 1.45 mm and 3.565×10^{-10} m^2 respectively. The profiles shown in Fig. 3 have been computed at 8 different positions along the pleat channels, namely X=5,10,15,20,25,30,40 and 45 mm and an average filtration velocity $\langle V_w\rangle=0.39$ m/s (which corresponds to Re_w=91.3 for δ=0.2, Re_w=60.9 for δ=0.8 and Re_0=1097.3). The profiles of the velocity longitudinal component $u(x,y)$ shown in Figs. 3a and b are for an impervious pleat bottom and a full porous one respectively. As can be seen from Fig. 3, the various profiles collapse reasonably well onto single curves close to the theoretical prediction (solid lines) deduced from Eqs. (1), (4)–(8) and (9)–(11). Similar results are obtained for the component $v(x,y)$, Rebai (2007). We conclude that we can rely on the similarity solutions proposed by Terrill (1965) to develop our flow model in the pleated filter element. Further validations of the relevance of this assumption are presented in Section 3.

3. One-dimensional flow model

The procedure used to develop the one dimensional flow model is similar to the one detailed in Oxarango et al. (2004). The important differences lie in the expression of the similarity solution, which is here the one corresponding to large suction or injection, and in the fact that channels of variable width are considered (as opposed to the uniform width system considered in Oxarango et al. (2004)). Details on the model derivation are given in Appendix B. As shown in Appendix B, the model can be summarized as

$$\frac{d\langle u_1\rangle}{dx}+\frac{1}{h_1}\frac{dh_1}{dx}\langle u_1\rangle+\frac{1}{h_1}\mathrm{Re}_0\,k\frac{\langle p_1\rangle-\langle p_2\rangle}{e}=0 \tag{14}$$

$$\frac{1}{2}\left[1-\frac{1}{2h_1}\left(1+\left(\frac{dh_1}{dx}\right)^2\right)\right]\frac{d\langle u_1\rangle^2}{dx}+\frac{1}{h_1}\frac{dh_1}{dx}\left[\frac{3}{2}-\frac{1}{h_1}\left(1+\left(\frac{dh_1}{dx}\right)^2\right)\right]\langle u_1\rangle^2-\frac{1}{h_1^2}\frac{1}{\mathrm{Re}_0}\left[h_1+1+\left(\frac{dh_1}{dx}\right)^2+h_1\frac{d^2h_1}{dx^2}\right]\langle u_1\rangle-\frac{1}{h_1}\frac{2}{\mathrm{Re}_0}\frac{dh_1}{dx}\frac{d\langle u_1\rangle}{dx}-\frac{1}{\mathrm{Re}_0}\frac{d^2\langle u_1\rangle}{dx^2}+\frac{d\langle p_1\rangle}{dx}=0 \tag{15}$$

$$\frac{d\langle u_2\rangle}{dx}+\frac{1}{h_2}\frac{dh_2}{dx}\langle u_2\rangle-\frac{1}{h_2}\,\mathrm{Re}_0\,k\frac{\langle p_1\rangle-\langle p_2\rangle}{e}=0 \tag{16}$$

$$\frac{\pi}{8}\frac{d\langle u_2\rangle^2}{dx}-\frac{1}{\mathrm{Re}_0}\frac{d^2\langle u_2\rangle^2}{dx^2}+\frac{3\pi^2}{16}\frac{1}{h_2}\frac{dh_2}{dx}\langle u_2\rangle^2-\frac{2}{\mathrm{Re}_0}\frac{1}{h_2}\frac{dh_2}{dx}\frac{d\langle u_2\rangle}{dx}+\frac{1}{h_2^2}\frac{1}{\mathrm{Re}_0}\left[\frac{\pi^2}{4}\left(1+\left(\frac{dh_2}{dx}\right)^2\right)-h_2\frac{d^2h_2}{dx^2}-\frac{\pi}{2}h_2\gamma\right]\langle u_2\rangle+\frac{d\langle p_2\rangle}{dx^2}=0 \tag{17}$$

where γ is a numerical constant, $\gamma\approx 0.8251$.

The above equations are to be solved in conjunction with the following boundary conditions:

$$\langle u_1\rangle=1,\ \langle u_2\rangle=0 \text{ at } x=0;\ \langle u_1\rangle=0,\quad \langle p_2\rangle=p_e \text{ at } x=\ell(\ell=L/H_0) \tag{18}$$

when the pleat bottom is considered as impervious or

$$\langle u_1\rangle+\langle u_2\rangle=1,\quad \langle u_2\rangle=\mathrm{Re}_0\frac{k}{e}(\langle p_1\rangle-\langle p_2\rangle) \text{ at } x=0 \tag{19}$$

$$\langle u_1\rangle+\langle u_2\rangle=1,\quad \langle u_1\rangle=\mathrm{Re}_0\frac{k}{e}(\langle p_1\rangle-\langle p_2\rangle),\quad \langle p_2\rangle=p_e \text{ at } x=\ell \tag{20}$$

when the pleat bottom is porous. Note that the permeability and fibrous material thickness in pleat bottoms can be chosen different from their values in the pleat bulk.

The system of Eqs. (14)–(18) or (14)–(17), (19),(20) are solved combining a finite difference method of discretization with a Newton–Raphson method (to deal with the non-linearities and the coupled nature of the system). Details can be found in Rebai (2007). Sensitivity study to the number of grid points has been carried out, considering up to 2500 equally spaced grid points. This study indicated that a grid of 200 up to 300 points was a good trade-off between accuracy and computational time. Typically, the time for computing the flow using the 1D model is on the order of one to two seconds on a standard Linux PC. This time is to be compared to the time of 5 min needed for a direct computation using the CFD commercial software on the same platform, without mentioning the time needed for preparing the CFD computation (grid construction, etc).

4. One-dimensional flow model validation

In order to validate the one-dimensional (1D) model, extensive comparisons with CFD computations using the commercial software have been carried out, Rebai (2007). On the whole, the agreement between the one-dimensional model results and the CFD direct simulations is very good. As representative examples of these results, Fig. 4 shows examples of comparison for the filtration velocity V_w along the pleat for a pleat element of uniform width (Fig. 4a) and for a pleat element of varying width (Fig. 4b). Details on each case shown in Fig. 4 are given in the figure caption. Note that the filtration velocity along the pleat is a key element in the perspective of clogging simulations. As can be seen from Fig. 4, the agreement between the direct CFD simulation and the 1D model is quite satisfactory for the uniform pleat and still better for the pleat element of varying width. The most noticeable differences occur in the pleat entrance (where the flow is not yet established contrary to what is assumed with the 1D model) and bottom region (where the filtration velocity becomes on the order of the average velocity in the channel). Also, as mentioned in the Introduction, Fig. 4 shows that the filtration velocity significantly varies along the pleat, which is a distinguishing feature of the air filtration problem considered here.

As an additional validation, comparisons have been made with experimental results. To this end, measurements of overall pressure drop through a pleated filter panel as a function of average filtration velocity (=flow rate/developed surface of filter panel) have been performed for various pleat lengths and pleat densities as well as for two different fibrous materials. Limited information on the experimental set-up is given in Appendix C. One can refer again to Rebai (2007) for more details on the experiments. Results of the comparison for one of the fibrous material (thickness E=1.45 mm, permeability $K=3.565\times10^{-10}$ m^2, measured by a specific experiment) are displayed in Fig. 5. The experimental results error bars correspond to the measurement uncertainties (flow rate and pressure drop). As can be seen from Fig. 5, the experimental results lie between the two curves obtained with the 1D model corresponding to the impervious pleat bottom case and full porous pleat bottom case, respectively. Hence, these results indicate that the pleat bottom hydraulic resistance is a quite sensitive parameter. It can be fitted so as to obtain an excellent agreement with the experimental results. This interesting result indicates that attention should be paid in the pleat making process for not altering too much the fibrous material transport properties in the pleat bottom if one is willing to minimize the overall hydraulic resistance of the pleated filter. This is especially important for systems operating at high filtration velocities, as shown in Fig. 5. Results obtained using the CFD commercial code are also shown in Fig. 5. Again, the agreement is very good between the 1D model and the direct CFD simulations. The differences between the experimental and the numerical results could also be explained in part by the overlap phenomenon pointed out and analysed in Subrenat et al. (2003), that is the formation of a dead zone in the pleat bottom region when the two porous walls forming the pleat come into contact before the pleat bottom. The effect will be somewhat similar to an apparent reduction of the pleat bottom permeability. This overlap phenomenon was not observed, however, with the filters used in the experiments but the observations were possible before and after the experiments but not during the experiments. Also, the pleat walls are locally deformed during the fabrication process and the little bumps resulting from the local deformations help the pleats maintain their shape. Hence we believe that the overlap phenomenon is negligible here. It would not be difficult, however, to take into account this effect with our model. This overlap phenomenon is indeed somewhat similar to the formation of a filtration cake from the pleat bottoms simulated and analysed in Rebai et al. (2009), which also leads to the formation of a (growing) dead zone in the pleat bottom.

From the results shown in this section, we conclude that the 1D model allows us to compute adequately the essential features of the flow in pleated filters for high filtration velocities. Key advantages of this model are the short computational times and the fact that a sensitivity analysis is easy to perform since no tedious grid generation is needed (as opposed to direct CFD simulation) for exploring for example the impact of pleat shape. This is illustrated in the next section devoted to a study of the optimal pleat density.

5. Optimal pleat density

Consider a filter panel of given frontal area and volume. We want to determine the pleat density (=number of pleats per 100 mm) that minimizes the pressure drop across the filter. The existence of an optimum is due to the fact that two effects contribute to the overall pressure drop. A first contribution results

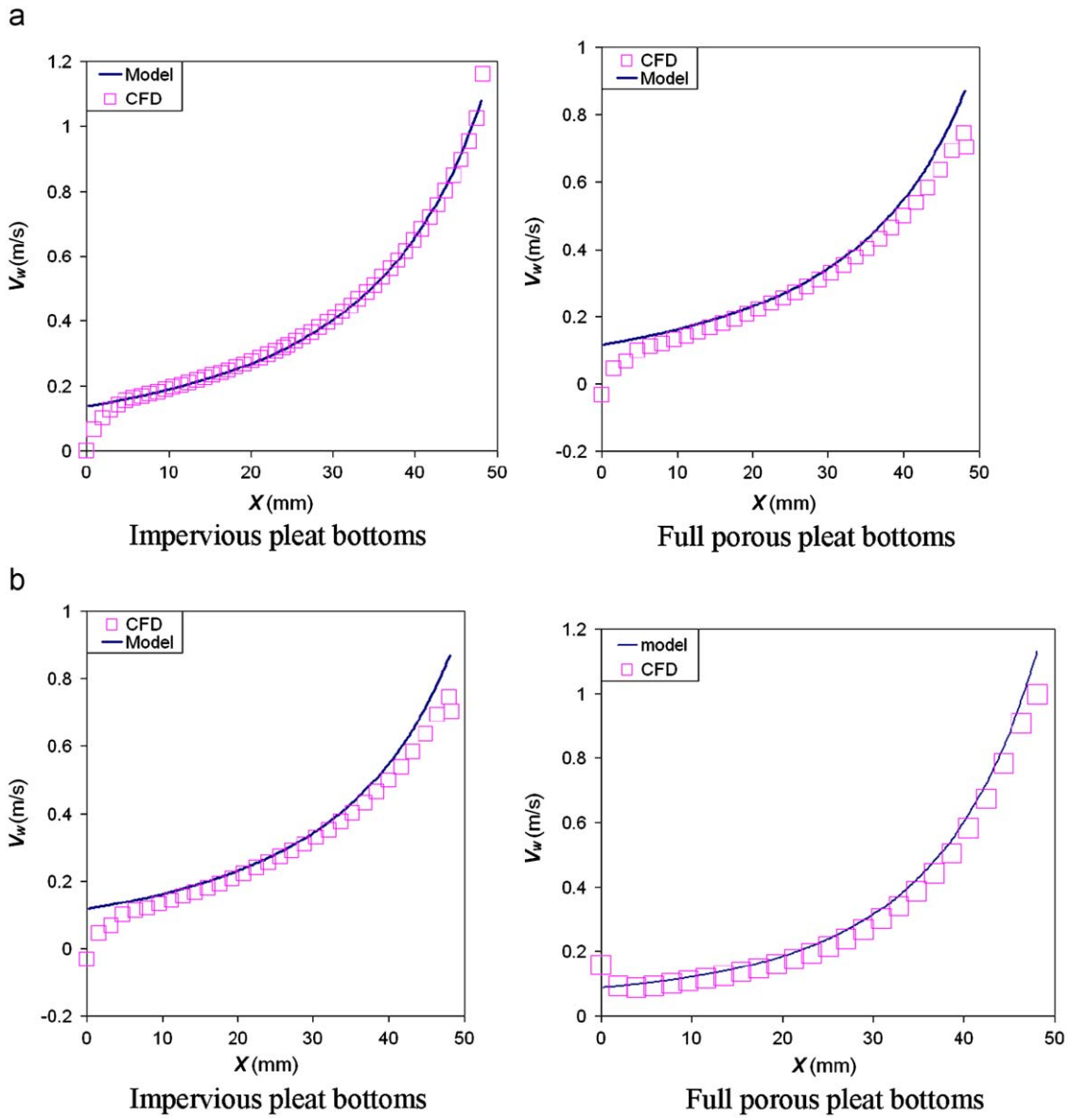

Fig. 4. Evolution of filtration velocity V_w along the pleat. Pleat density is 8 pleats per 100 mm and the pleat height is 51 mm: (a) δ=1.0 (H_0=3.125 mm, $\delta=H_s/H_0$). The averaged filtration velocity $\langle V_w \rangle$ is 0.40 m/s (filtration Reynolds number $Re_w \approx 73$, pleat Reynolds number $Re_0 \approx 1126$). (b) δ=0.8 (H_0=2.67 mm). The averaged filtration velocity is 0.39 m/s (filtration Reynolds number $Re_w \approx 60$, pleat Reynolds number $Re_0 \approx 1097$).

from the filtration flow through the filter (porous) medium. According to Darcy's law, the pressure drop increases linearly with the filtration velocity. If this effect was the only one to take into consideration, it would imply to maximize the filtration area, i.e. the pleat density, for minimizing the pressure drop. The second contribution to the overall pressure drop is due to the flow within the pleat channels where viscous as well as inertial effects contribute to the pressure drop. As regards this second contribution, the more the fibrous medium is pleated, the higher the pressure drop. Thus increasing the pleat length and pleat density increases the pressure drop due to the flow in the channels. Hence, maximizing the pleat density increases the second contribution. Therefore, there should be some trade-off between these two contributions, i.e. the one due to the flow across the fibrous medium and the one due to the flow in the pleat channels so as to minimize the overall pressure drop.

This problem has been previously considered by several authors, i.e. Raber (1982), Yu and Goulding (1992), Chen et al. (1995), Lücke and Fissan (1996), Del Fabbro (2001), Del Fabbro et al. (2002) but for average filtration velocities much lower than the ones considered in the present work. As pointed out in their paper, the model of Lücke and Fissan (1996) becomes in error for high filtration velocities and therefore cannot be expected to give good results in our case (one reason for this is that the channels velocity profiles are not parabolic in our case, contrary to what is assumed in Lücke and Fissan model). This holds also for the models proposed by Chen et al. (1995). A dimensionless model for pleat optimization is proposed in Del Fabbro (2001). The "model" proposed by Del Fabbro is in fact an empirical correlation fitted over a series of experimental results corresponding to low filtration velocities. It is therefore expected that this correlation leads to poor predictions for filtration velocities significantly different from the filtration velocity range of calibration. This is illustrated in Fig. 6 where the results obtained with our 1D model are compared, for high filtration velocity conditions, with predictions using Del Fabbro's correlation as well as with a few

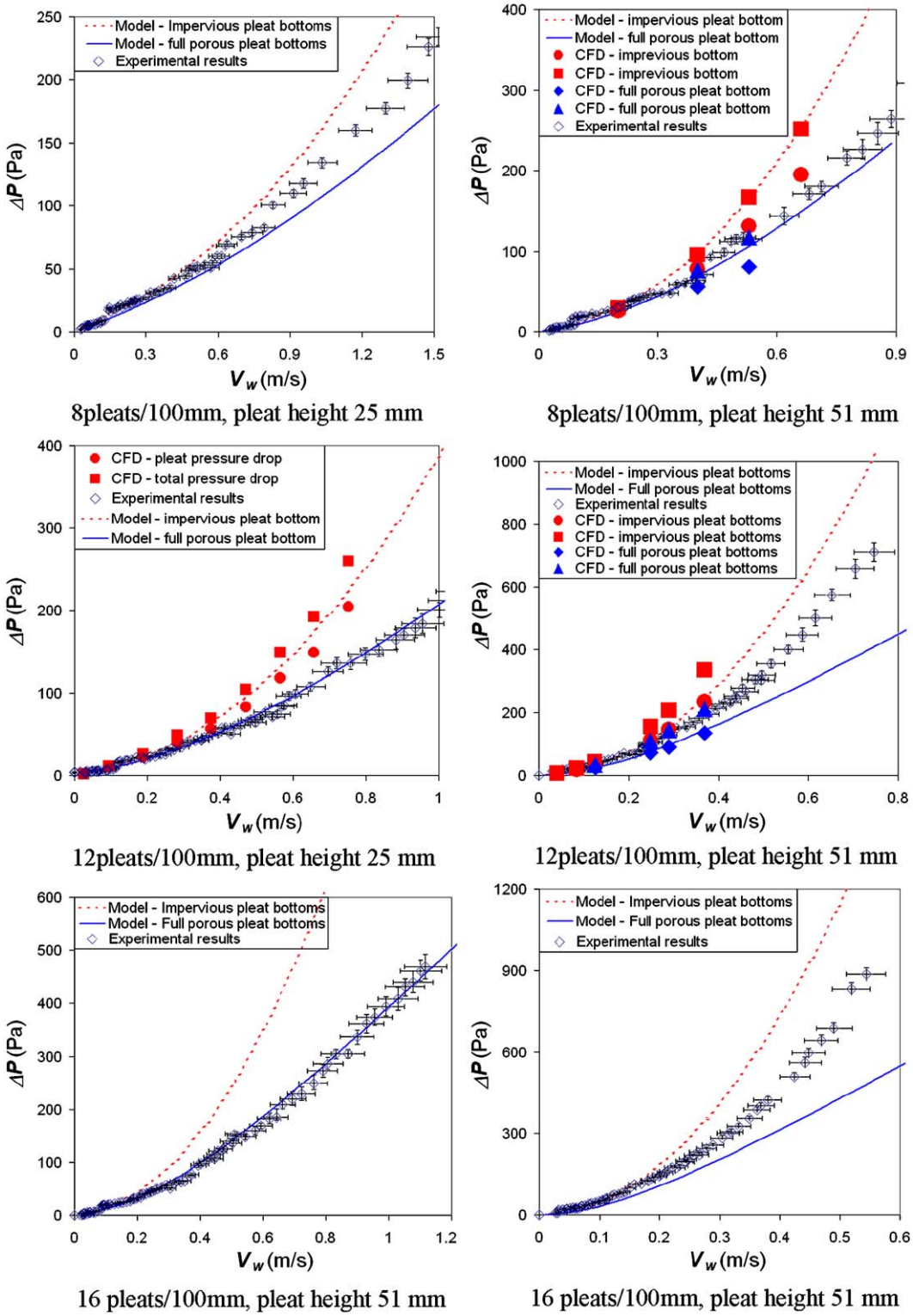

Fig. 5. Evolution of the pressure drop ΔP as a function of averaged filtration velocity (noted V_w instead of $\langle V_w \rangle$ in the figure for simplicity) for different pleated filter configurations. Comparison between 1D model (solid and dashed lines), experimental results and some CFD results (circles and diamonds for the pressure drop across the pleat; squares and triangles for the total pressure drop, i.e. the pressure drop across the pleat together with the entrance and exit pressure drops due to the flow contraction (pleat entrance) and expansion (pleat exit)).

experimental results, obtained using the same experimental facility as for the results presented in Section 3. Two different flows rates were investigated: 0.108 and 0.160 m^3/s. All pleated filters have the same frontal surface (220 mm × 89 mm $= 1.985 \times 10^{-2}\,m^2$), pleat height (55 mm) and fibrous medium properties (thickness $E = 2.85$ mm and permeability $K = 2.28 \times 10^{-10}\,m^2$). Not surprisingly, Del Fabbro's correlation leads to poor results here and cannot capture the optimum. Although it would have been interesting to have experimental results also for lower pleat densities so as to locate the optimum experimentally, a good agreement can be observed between our 1D model and the available experimental data. An interesting result also emerges

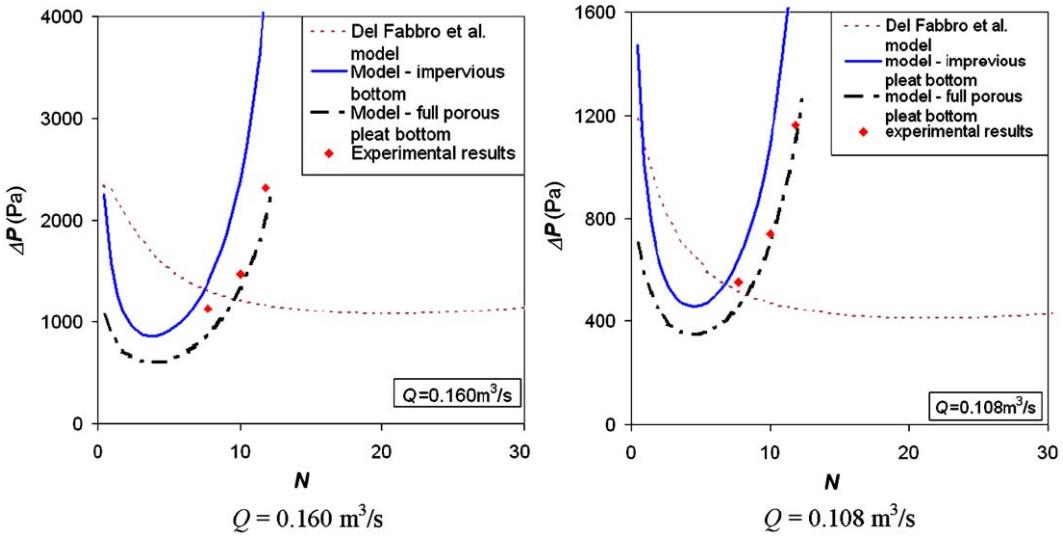

Fig. 6. Evolution of pleated filter overall pressure drop ΔP with the pleat density N (pleat number/100 mm). These results are for a pleated filter of frontal area of 220 mm × 89 mm (0.01958 m^2) and pleat height of 55 mm. The thickness of filter medium is 2.85 mm and its permeability is 2.28×10^{-10} m^2. Q is the flow rate through the filter.

from the results shown in Fig. 6. The optimum pleat density is the same regardless of the impervious or porous nature of the pleat bottoms. Hence even though there exists some uncertainty regarding the fibrous material characteristics (thickness, permeability) in the pleat bottom regions, this does not affect the identification of the optimal pleat density. Also, the results shown in Fig. 6 indicate that the optimum pleat density tends to diminish with the flow rate since the optimum pleat density is 4 pleats/100 mm and 5 pleats/100 mm for 0.160 and 0.108 m^3/s respectively. This result seems to disagree with the results of Yu and Goulding (1992) and Chen et al. (1995) which are independent of the flow rate. However, this difference can be explained by the influence of inertia effects in the pleat as shown in Appendix D, see also Li (2009). The optimal pleat density was discussed here for a given height of 55 mm. It is clear that both pleat density and pleat height should be considered in parallel when optimizing a filter design. Our model is clearly well adapted to investigate the interrelationship between the pleat density and pleat height minimizing the pressure drop.

6. Conclusion

A semi-analytical model was proposed to calculate the flow in an element of a pleated filter for the high filtration velocities representative of gas filtration in automobile applications. This case presents two main distinguishing features compared to the low filtration velocity situations studied in previous works: the velocity profiles are not parabolic within the pleat channels and the filtration velocity is not uniform along the pleated filter element. The model relies on similarity solutions to the Navier–Stokes equations and has been validated by comparison with direct CFD simulations and experimental data.

The model is much easier to use and much less computational time demanding than a standard CFD software. For this reason, it greatly facilitates the sensitivity studies and can be used as a design-sizing tool to limit for example the number of trials in the development of a filter. This has been illustrated in the present work by determining the pleat density minimizing the pressure drop across the filter element for a given flow rate.

This model forms a good basis for the modelling and the study of clogging. The model is applicable to depth filtration media and surface filtration media by combining it to a surface and depth filtration model (describing the capture of particles at the scale of the filter medium), see Rebai et al. (2009) for an example. In particular, it is fairly easy with this model to take into account the variations in permeability due to the depth filtration as well as the variations in the entrance channel aperture due to the cake formation at the channel walls Rebai (2007), Rebai et al. (2009). Also, no remeshing is needed across the channel width when a filtration cake forms at the channel walls, a decisive advantage compared to direct CFD approaches As reported in Rebai (2007), Rebai et al. (2009), the fact that the filtration velocity is not uniform along the pleated filter element for the high filtration velocities has important effects on the filter loading. These aspects are presented and discussed in Rebai et al. (2009).

Notation

d_f	fibre diameter, m
e	dimensionless porous medium thickness, $e=L/H_0$
E	porous medium thickness, m
f	similarity function
$h(x)$	dimensionless local channel half width
H_0	channel half-width at entrance (resp. exit) channel inlet (resp. outlet), m
H_s	channel half-width at entrance (resp. exit) channel end (resp. inlet), m
k	dimensionless porous medium permeability, $k=K/H_0/H_0$
K	porous medium permeability (m^2)
ℓ	dimensionless pleat length, $\ell = L/H_0$
L	pleat length, m
N	pleat density (pleat number/100 mm)
p	dimensionless pressure, $p = P/\rho\langle U_0\rangle^2$
P	Pressure, Pa
ΔP	overall filter pressure drop, Pa
Q	flow rate, m^3/s
u	dimensionless x component of velocity vector

$\mathbf{u}$	dimensionless velocity vector
$\langle U_0 \rangle$	average longitudinal velocity at the entrance channel inlet, m/s
U	x component of velocity vector, m/s
v	dimensionless y component of velocity vector
V	y component of velocity vector, m/s
V_w	filtration velocity, m/s
$\langle V_w \rangle$	average filtration velocity, m/s
x	dimensionless spatial coordinate
X	spatial coordinate, m
y	dimensionless spatial coordinate
Y	spatial coordinate, m
z	reduced spatial coordinate, $z=1-y/h(x)$ or $z=(\pi/2)(y/h)$

Greek letters

$\delta = H_s/H_0$	
$\varepsilon = -\pi/2\,\mathrm{Re}_w$	
μ	dynamic viscosity, Pa s
ρ	fluid density, kg/m^3
Φ	filtration medium porosity

Dimensionless numbers

Re_f	fibre Reynolds number, $\mathrm{Re}_f = \rho d_f \langle V_w \rangle / \phi\mu$
Re_0	channel Reynolds number, $\mathrm{Re}_0 = \rho \langle U_0 \rangle H_0/\mu$
Re_w	filtration Reynolds number, $\mathrm{Re}_w = \rho \langle V_w \rangle H_0/\mu$

Subscripts

Subscript 1 is for the entrance channel	
Subscript 2 is for the exit channel	

Appendix A. CFD simulations

An example of computational domain used for the direct CFD simulations is shown in Fig. A1 (for the case of channels of uniform width). As can be seen from Fig. A1, the computational domain is longer than the pleated filter element so as to include flow entrance and exit zones upward and downward the filter element. The boundary conditions read (with U_n and U_t denoting the velocity components normal and tangential to a boundary respectively):

- West (entrance): $U_n = (H_0/(2H_0+E))U_0$, U_t=0;
- East (exit): outlet condition $\partial^2 U_n/\partial t^2 = 0$, $\partial^2 U_t/\partial t^2 = 0$.
- North and South: symmetry conditions: $U_n = 0$, $\partial U_t/\partial n = 0$, $\partial U_n/\partial n = 0$, $\partial P/\partial n = 0$;
- Wall: no-slip boundary condition: $U_t = 0$, $U_n = 0$;
- Interface: no condition imposed.

A momentum source of the form $S_i = \mu \sum_{j=1}^{3} (1/K_{ij}) u_j$ is added to the Navier–Stokes equations in the porous domain. Hence, for a homogeneous porous medium, the equation solved in the porous region reads $\mathbf{u}\cdot\nabla\mathbf{u} = -\nabla p + (1/\mathrm{Re}_0)\nabla^2\mathbf{u} - (1/\mathrm{Re}_0)\mathbf{u}/k$.

We have used grids containing 41 000–126 000 meshes over the whole computational domain depending on the pleat geometry and flow rate. At least eleven grid points were located over the porous medium thickness. A flow recirculation takes place in the zone located right after the exit channel due to the expansion of the flow. It is necessary to have locally fine meshes with edge ratio close to one in this area in order to ensure a good convergence of calculations. The mesh type used was Quad/Pave.

Appendix B. Derivation of 1D flow model

The procedure begins with the differentiation of Eqs. (1) and (2). Since the channel half-width h depends on the position x, this leads to:

$$\frac{\partial u}{\partial x} = \frac{d\langle u\rangle}{dx} f'\left(\frac{y}{h}\right) - \frac{y}{h^2}\frac{dh}{dx} f''\left(\frac{y}{h}\right)\langle u\rangle \tag{B.1}$$

$$\frac{\partial v}{\partial y} = \frac{1}{h}\frac{\mathrm{Re}_w}{\mathrm{Re}_0} f'\left(\frac{y}{h}\right) \tag{B.2}$$

For two dimensional Cartesian coordinates, substituting Eqs. (B.1) and (B.2) into Eq. (12) gives,

$$\frac{d\langle u\rangle}{dx} f'\left(\frac{y}{h}\right) - \frac{y}{h^2}\frac{dh}{dx} f''\left(\frac{y}{h}\right)\langle u\rangle + \frac{1}{h}\frac{\mathrm{Re}_w}{\mathrm{Re}_0} f'\left(\frac{y}{h}\right) = 0 \tag{B.3}$$

Eq. (B.3) is then averaged on half-width of the channel. This yields

$$\frac{d\langle u\rangle}{dx} + \frac{1}{h}\frac{dh}{dx}\langle u\rangle + \frac{1}{h}\frac{\mathrm{Re}_w}{\mathrm{Re}_0} = 0 \tag{B.4}$$

The same method as for Eqs. (B.1) and (B.2) is used to determine $\partial u/\partial y$, $\partial^2 u/\partial x^2$ and $\partial^2 v/\partial y^2$ from Eqs. (1) and (2). Those results are substituted into Eq. (13). The result, is then combined with equation (B.4) and after averaging over the channel half-width, one obtains,

$$\begin{aligned}\frac{1}{2}\left[\int_0^1 (f'^2 - f''f)\,dz\right]\frac{d\langle u\rangle^2}{dx} + \frac{1}{2}\left[\int_0^1 (f'^2 - 2f''f)\,dz\right]\frac{1}{h}\frac{dh}{dx}\langle u\rangle^2 \\ - \frac{1}{\mathrm{Re}_0} f''(1)\frac{\langle u\rangle}{h^2} - \frac{1}{\mathrm{Re}_0}\frac{d^2\langle u\rangle}{dx^2} - \frac{2}{\mathrm{Re}_0}\frac{1}{h}\frac{dh}{dx}\frac{d\langle u\rangle}{dx} - \frac{1}{\mathrm{Re}_0}\frac{1}{h}\frac{d^2h}{dx^2}\langle u\rangle \\ - \frac{1}{\mathrm{Re}_0}\frac{1}{h^2}\frac{dh}{dx}\left(2 + f''(1) - 2\frac{dh}{dx}\right)\langle u\rangle + \frac{d\langle p\rangle}{dx} = 0\end{aligned} \tag{B.5}$$

Eq. (B.5) is the one dimensional momentum conservation equation for a pleated channel of variable width. To obtain the

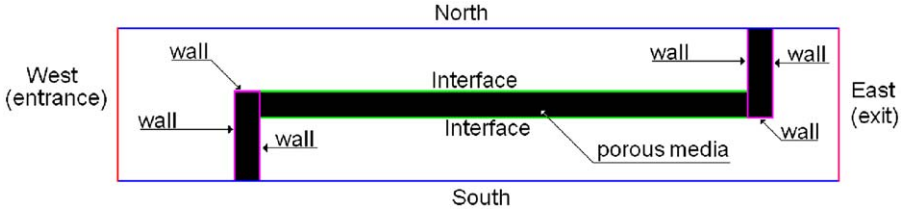

Fig. A1

equation for the entrance (resp. exit) channel, integrals

$$\int_0^1 (f'^2 - f''f)\,dz \quad \text{and} \quad \int_0^1 (f'^2 - 2f''f)\,dz$$

as well as $f''(1)$ have to be evaluated using Eqs. (4)–(7) (resp. Eqs. (8)–(10) for exit channel). Both integrals are determined by the same method. We only present the method for one of them for the entrance and exit channel.

$$\int_0^1 (f'^2 - f''f)\,dz$$

is determined for entrance channel using Eqs. (4)–(7) at the second order:

$$\int_0^1 (f'^2 - f''f)\,dz = -\frac{1}{\mathrm{Re}_w - 1}\int_0^1 f_1''\,dy + \frac{1}{(\mathrm{Re}_w-1)^2}\int_0^1 [f_1'^2 - f_2'' - f_1''f_1]\,dy \tag{B.6}$$

Using Taylor expansion series at the second order in $1/\mathrm{Re}_w$, and substituting the result into Eq. (B.5) gives

$$\frac{1}{2}\left[1-\frac{1}{2h}\left(1+\left(\frac{dh}{dx}\right)^2\right)\right]\frac{d\langle u\rangle^2}{dx} + \frac{1}{h}\frac{dh}{dx}\left[\frac{3}{2}-\frac{1}{h}\left(1+\left(\frac{dh}{dx}\right)^2\right)\right]\langle u\rangle^2 - \frac{1}{h^2}\frac{1}{\mathrm{Re}_0}\left[h+1+\left(\frac{dh}{dx}\right)^2 + h\frac{d^2h}{dx^2}\right]\langle u\rangle - \frac{2}{\mathrm{Re}_0}\frac{1}{h}\frac{dh}{dx}\frac{d\langle u\rangle}{dx} - \frac{1}{\mathrm{Re}_0}\frac{d^2\langle u\rangle}{dx^2} + \frac{d\langle p\rangle}{dx} = 0 \tag{B.7}$$

Hence the system of one dimensional equations governing the flow in the entrance channel with non-uniform aperture reads,

$$\begin{cases} \dfrac{d\langle u_1\rangle}{dx} + \dfrac{1}{h_1}\dfrac{dh_1}{dx}\langle u_1\rangle + \dfrac{1}{h_1}\dfrac{\mathrm{Re}_{w_1}}{\mathrm{Re}_0} = 0 \\ \dfrac{1}{2}\left[1-\dfrac{1}{2h_1}\left(1+\left(\dfrac{dh_1}{dx}\right)^2\right)\right]\dfrac{d\langle u_1\rangle^2}{dx} + \dfrac{1}{h_1}\dfrac{dh_1}{dx}\left[\dfrac{3}{2}-\dfrac{1}{h_1}\left(1+\left(\dfrac{dh_1}{dx}\right)^2\right)\right]\langle u_1\rangle^2 \\ \qquad -\dfrac{1}{h_1^2}\dfrac{1}{\mathrm{Re}_0}\left[h_1+1+\left(\dfrac{dh_1}{dx}\right)^2 + h_1\dfrac{d^2h_1}{dx^2}\right]\langle u_1\rangle \\ \qquad -\dfrac{2}{\mathrm{Re}_0}\dfrac{1}{h_1}\dfrac{dh_1}{dx}\dfrac{d\langle u_1\rangle}{dx} - \dfrac{1}{\mathrm{Re}_0}\dfrac{d^2\langle u_1\rangle}{dx^2} + \dfrac{d\langle p_1\rangle}{dx} = 0 \end{cases} \tag{B.8}$$

where subscript 1 refers to the entrance channel (or channel 1).

Since the comparison between the outer solution, Eqs. (8)–(10), and the CFD results are in good agreement as far as the exit channel is concerned, Figs. 4a and b, only the outer solution has been used. Therefore, using Eqs. (8)–(10) to determine the following integral

$$\int_0^1 (f'^2 - f''f)\,dz$$

leads to:

$$\int_0^1 (f'^2 - f''f)\,dz = \int_0^1 (f_0'' - f_0''f_0)\,dz + \varepsilon\int_0^1 (f_0'f_1' - f_0''f_1 - f_0f_1'')\,dz \tag{B.9}$$

Substituting Eq. (B.9) in momentum conservation Eq. (B.5) and using Eqs. (8)–(10) yield,

$$\frac{\pi^2}{8}\frac{d\langle u\rangle^2}{dx} - \frac{1}{\mathrm{Re}_0}\frac{d^2\langle u\rangle}{dx^2} + \frac{d\langle p\rangle}{dx} + \frac{3\pi^2}{16}\frac{1}{h}\frac{dh}{dx}\langle u\rangle^2 - \frac{2}{\mathrm{Re}_0}\frac{1}{h}\frac{dh}{dx}\frac{d\langle u\rangle}{dx} + \frac{1}{\mathrm{Re}_0}\frac{1}{h^2}\left[\frac{\pi^2}{4}\left(\left(\frac{dh}{dx}\right)^2+1\right) - h\frac{d^2h}{dx^2} - \frac{\pi}{2}h\gamma\right]\langle u\rangle = 0 \tag{B.10}$$

where γ is a numerical constant resulting from the integration procedure, $\gamma \approx 0.8251$.

Hence the system of one dimensional equations governing the flow in the exit channel with non-uniform aperture reads

$$\begin{cases} \dfrac{d\langle u_2\rangle}{dx} + \dfrac{1}{h_2}\dfrac{dh_2}{dx}\langle u_2\rangle + \dfrac{1}{h_2}\dfrac{\mathrm{Re}_{w_2}}{\mathrm{Re}_0} = 0 \\ \dfrac{\pi^2}{8}\dfrac{d\langle u_2\rangle^2}{dx} - \dfrac{1}{\mathrm{Re}_0}\dfrac{d^2\langle u_2\rangle}{dx^2} + \dfrac{3\pi^2}{16}\dfrac{1}{h_2}\dfrac{dh_2}{dx}\langle u_2\rangle^2 - \dfrac{2}{\mathrm{Re}_0}\dfrac{1}{h_2}\dfrac{dh_2}{dx}\dfrac{d\langle u_2\rangle}{dx} \\ \qquad + \dfrac{1}{\mathrm{Re}_0}\dfrac{1}{h_2^2}\left[\dfrac{\pi^2}{4}\left(\left(\dfrac{dh_2}{dx}\right)^2+1\right) - h_2\dfrac{d^2h_2}{dx^2} + \dfrac{\pi}{2}h_2\gamma\right]\langle u_2\rangle + \dfrac{d\langle p_2\rangle}{dx} = 0 \end{cases} \tag{B.11}$$

where subscript 2 refers to the exit channel (or channel 2).

The Reynolds number of filtration Re_{w_1} and Re_{w_2} depend on the filtration velocity through the porous media. Thus we have 4 equations for the 6 unknowns: $\langle u_1\rangle$, $\langle u_2\rangle$, $\langle p_1\rangle$, $\langle p_2\rangle$, Re_{w_1} and Re_{w_2}. The coupling between entrance and exit channel gives the missing equations. To this end, we assume that: (i) the flow inside the porous media is perpendicular to the surface and that the flow inside the medium along the medium can be neglected, (ii) the flow inside the porous medium obeys Darcy's law:

$$\nabla P = -\frac{\mu}{K}U \tag{B.12}$$

Assumption (i) and the mass conservation inside the porous medium lead to:

$$V_{w_1}(x) = -V_{w_2}(x) = V_w(x) \tag{B.13}$$

As we assume that the flow in the porous media is only in the direction perpendicular to the medium, we have from Darcy's law,

$$V_w = \frac{K}{\mu}\frac{\Delta P}{E} \tag{B.14}$$

where ΔP is the pressure drop across the porous medium thickness.

Moreover, as the pressure is uniform in each channel cross-section, the pressure at the channel/porous media interface is then the same as the cross-section average pressure in the channel:

$$\Delta P = \langle P_2\rangle - \langle P_1\rangle \tag{B.15}$$

Using Eq. (B.15) Eq. (B.14) is expressed in dimensionless form as

$$\frac{\mathrm{Re}_w}{\mathrm{Re}_0} = \mathrm{Re}_0 k\frac{\langle p_2\rangle - \langle p_1\rangle}{e} \tag{B.16}$$

Appendix C. Experimental set-up

Fig. C1 shows a schematic diagram of the experimental set-up. It consists of a chamber with a filter holder containing the test filter, two pressure sensors upstream and downstream and a critical orifice. Temperature is controlled so as to determine the volumetric flow rate from the mass flow rate measured with the critical orifice. The chamber is of rectangular shape. Small holes are drilled on each side of the chamber upstream and downstream of the filter holder for measuring the upstream and downstream static pressure. The pleated medium is fixed on the filter holder so as to avoid any parasitic gas leakage and therefore to force the gas flow through the filter medium. The air flow is generated in the system thanks to an aspiration pump (not shown in Fig. C1). The pressure difference and the flow rate are measured for various aspiration flow rates so as to cover the range of average filtration velocities of interest (see Fig. 5).

Three types of experiments were performed to study gas flow in pleated filter panels:

(i) A series of experiments using round samples of fibrous material were first performed to determine the permeability

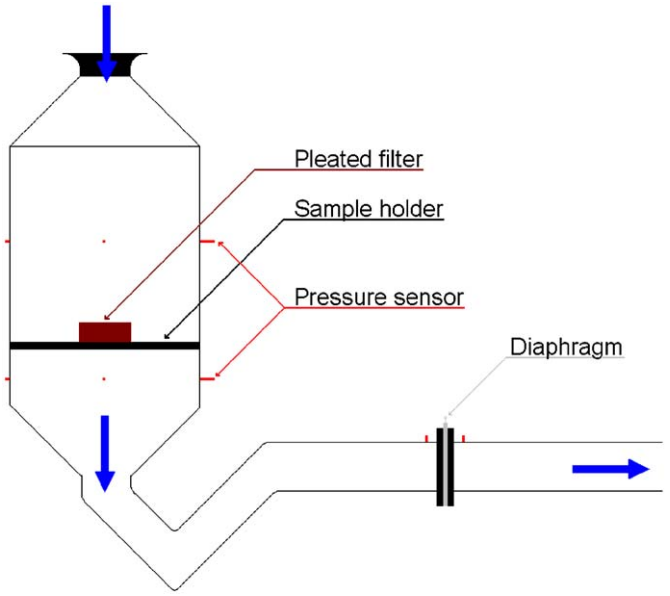

Fig. C1. Sketch of experimental set-up.

Table C1
Geometrical characteristics of pleated filter panels.

Number of pleats	Length (mm)	Width (mm)	Height (mm)	Pleat density (number/100 mm)
33	412	180	25	8
16	200	180	51	8
33	275	180	25	12
16	133	180	51	12
33	206	180	25	16
16	100	180	51	16

of the media. The sample areas were the following: 100, 50, 20 and 5 cm^2. A large range of filtration velocities were chosen from 0.1 m/s to 1.5 m/s.

(ii) Rectangular samples of pleated filter panels were used to get experimental data for semi-analytical model validation (Section 4). The net filtration area is the same for all the samples. The characteristics of the different samples used are written in Table C1.

(iii) Rectangular samples of pleated filter panels of the same frontal area (220 mm × 89 mm) were used to study the optimal pleat density (Section 5).

The whole experiments were done in Mecaplast research center, Lens, France. All the instruments are periodically verified and certified by COFRAC association (www.cofrac.fr). The measurements were made with respect to ISO 9237 standards. The maximum relative error is ±2% for pressure measurements and ±4% for flow rate measurements.

Appendix D. Influence of flow rate on optimum pleat number

When inertia effects can be neglected, the pressure drop across the pleated filter is proportional to the filtration velocity as stated by Chen et al. (1995), i.e.

$$\Delta P = \alpha \langle V_w \rangle \tag{D.1}$$

where α depends on the porous medium and pleating characteristics (i.e. pleat number N), cf. Chen et al. (1995) for details about α. The filtration velocity can be expressed as functions of the filtration area S_f and the flow rate Q as $\langle V_w \rangle = Q/S_f$. This gives,

$$\Delta P = \frac{\alpha}{S_f} Q \tag{D.2}$$

Since the optimum pleat number corresponds to the minimization of the pressure drop ΔP, the optimum pleat number is given by the equation $\partial \Delta P/\partial N = 0$. Using (D.2) and noting that Q is constant this condition can be expressed as

$$\frac{\partial\left(\frac{\alpha}{S_f}\right)}{\partial N} = 0 \tag{D.3}$$

which does not depend on the flow rate.

When the inertia effects are taken into account Eq. (D.1) becomes

$$\Delta P = \alpha \langle V_w \rangle + \beta \langle V_w \rangle^2 \tag{D.4}$$

where β depends on the porous medium and pleating characteristics (and pleat number N), cf. Rebai (2007) for details about α and β in this case. This yields

$$\Delta P = \left(\frac{\alpha}{S_f} + \frac{\beta}{S_f^2} Q\right) Q \tag{D.5}$$

The optimum pleat number, which still corresponds to the minimization of pressure drop, is then given by the solution of the following equation:

$$\frac{\partial\left(\frac{\alpha}{S_f} + \frac{\beta}{S_f^2} Q\right)}{\partial N} = 0 \tag{D.6}$$

Contrary to Eqs. (D.3), (D.6) depends on the flow rate and not only on the filter medium and pleats characteristics.

References

Benmachou, K., Schmitz, P., Meireles, M., 2003. Dynamical clogging of a pleated filter: experimental and theoretical approaches for simulation. Filtech Europa 2, 51–57.
Benmachou, K., 2005. Etude et modélisation du colmatage d'un filtre plissé. Ph.D. Thesis, Institut National Polytechnique de Toulouse.
Berman, A.S., 1954. Laminar flow in channels with porous walls. Journal of Applied Physics 24 (9), 1232–1235.
Brady, J.F., 1984. Flow development in a porous channel and tube. Physics of Fluids 27 (5), 1061–1067.
Chen, D.R., Pui, D.Y.H., Liu, B.Y.H., 1995. Optimisation of pleated filter designs using a finite-element numerical model. Aerosol Science and Technology 23, 579–590.
Del Fabbro, L., Laborde, J.C., Merlin, P., Ricciadi, L., 2002. Air flows and pressure drop modelling for different pleated industrial filters. Filtration+Separation, 34–40.
Del Fabbro, L., 2001. Modélisation des écoulements d'air et du colmatage des filtres plissés par des aérosols solides. Ph.D. Thesis, Université Paris XII.
Dullien, F.A.L., 1992. Porous Media: Fluid Transport and Pore Structure, second ed. Academic Press, New York.
Li, C.C., 2009. Aerodynamic behavior of a gas mask canister containing two porous media. Chemical Engineering Science 64 (8), 1832–1843.
Lücke, T., Fissan, H., 1996. The prediction of filtration performance of high efficiency gas filter element. Chemical Engineering Science 51, 1199–1208.
Nassehi, V., Hanspal, N.S., Waghode, A.N., Ruziwa, W.R., Wakeman, R.J., 2005. Finite-element modelling combined free/porous flow regimes: simulation of flow through pleated cartridge filters. Chemical Engineering Science 60, 995–1006.
Oxarango, L., Schmitz, P., Quintard, M., 2004. Laminar flow in channels with wall suction or injection: a new model to study multi-channel filtration systems. Chemical Engineering Science 59, 1039–1051.
Raber, R.R., 1982. Pressure drop optimization and dust capacity estimation for a deep-pleated industrial air filter using small sample data. In: Proceedings of World Filtration Congress III, 52.
Rebai, M., Prat, M., Meireles, M., Schmitz, P., Baclet, R., 2009. Clogging modeling in pleated filters for gas filtration. Chemical Engineering Research and Design doi:10.1016/j.cherd.2009.08.014.
Rebai, M., 2007. Analyse et modélisation du colmatage d'un filtre plissé au sein d'un filtre à air plissé. Ph.D. Thesis, Institut National Polytechnique de Toulouse.

Subrenat, A., Bellettre, J., Le Cloirec, P., 2003. 3D numerical simulations of flow in a cylindrical pleated filter packed with activated carbon cloth. Chemical Engineering Science 58, 4965–4973.

Terrill, R.M., 1964. Laminar flow in a uniformly Porous channel. The Aeronautical Quaterly 15, 299–310.

Terrill, R.M., 1965. Laminar flow in a uniformly porous channel with large injection. The Aeronautical Quaterly 16, 323–332.

Yu, H.H.S., Goulding, C.H., 1992. Optimized ultra high efficiency filter for high-efficiency industrial combustion turbines. In: ASME International Gas Turbine and Aeroengine Congress and Exhibition, Köln.